PROCEEDINGS OF SPIE
SPIE—The International Society for Optical Engineering

Photon Management

Frank Wyrowski
Chair/Editor

27–28 April 2004
Strasbourg, France

Sponsored and Published by
SPIE—The International Society for Optical Engineering

Cooperating Organizations
EOS—European Optical Society (United Kingdom)
SFO—Société Française d'Optique (France)
SIOF—Società Italiana di Ottica e Fotonica (Italy)
DGaO—Deutsche Gesellschaft für angewandte Optik (Germany)
IEE—The Institution of Electrical Engineers
Photonics Clusters (United Kingdom)
oe*magazine*
NEMO—Network of Excellence in Micro-Optics

Supported by
Région Alsace (France)
Communauté Urbaine de Strasbourg (France)
Conseil Général du Bas-Rhin (France)
Alsace Development Agency (France)
European Office of Aerospace Research and Development,
U.S. Air Force Office of Scientific Research

Volume 5456

The papers included in this volume were part of the technical conference cited on the cover and title page. Papers were selected and subject to review by the editors and conference program committee. Some conference presentations may not be available for publication. The papers published in these proceedings reflect the work and thoughts of the authors and are published herein as submitted. The publisher is not responsible for the validity of the information or for any outcomes resulting from reliance thereon.

Please use the following format to cite material from this book:

Author(s), "Title of Paper," in *Photon Management*, edited by Frank Wyrowski, Proceedings of SPIE Vol. 5456 (SPIE, Bellingham, WA, 2004) page numbers.

ISSN 0277-786X
ISBN 0-8194-5383-8

Published by
SPIE—The International Society for Optical Engineering
P.O. Box 10, Bellingham, Washington 98227-0010 USA
Telephone 1 360/676-3290 (Pacific Time)· Fax 1 360/647-1445
http://www.spie.org

Printed in the United States of America.

Space-variant image processing with volume holography

A. Márquez[1,*], C. Neipp[1], S. Gallego[2], M. Ortuño[2], A. Beléndez[1] and I. Pascual[2]

[1]Depto. de Física, Ingeniería de Sistemas y Teoría de la Señal, Universidad de Alicante
[2]Departamento Interuniversitario de Óptica, Universidad de Alicante

ABSTRACT

In this work we explore the application of volume effects given by holographic optical elements (HOEs) to image processing operations. Bragg diffraction, exhibited by HOEs, modifies the impulse response of an imaging system, facilitating spatial filtering operations with no need for a physical Fourier plane. Both the holographic recording material we use and the specific HOE we design are important parameters. In the present communication we report our last results using a polyvinyl alcohol/acrylamide (PVA/AA) photopolymer. This compound combines good optical properties, ease of fabrication, and self-development capability. We are able to produce layers as thick as 1 millimeter (mm) with a diffraction efficiency higher than 80%. Using layers with a thickness of 0.1 mm and 1 mm we have recorded both holographic diffraction gratings and holographic lenses. When using the holographic gratings we can obtain image edge enhancement as demonstrated in previous works. As a novelty, in this work we show that when using the holographic lenses we obtain a space-variant image edge enhancement. We analyse the properties of this space-variant operation in terms of the reconstruction geometry and the local grating structure exhibited by the lens across its aperture.

Keywords: Optical image processing, holographic optical elements, space-variant imaging, Bragg diffraction, photopolymer.

1. INTRODUCTION

Volume holography[1] has been the subject of intensive research since the introduction of the laser in the 60s. The very specific properties of angular and wavelength selectivity given by Bragg diffraction offer unique capabilities, enabling applications with a great potential such as holographic data storage[2], holographic optical elements (HOEs)[3] and holographic interferometry[4]. One key point in volume holography is the availability of recording materials gathering the very demanding specifications usually required by most of the applications. Photopolymers are one of the most promising materials for write-once read-many (WORM) holographic memories and for HOEs, due to the great flexibility in their composition and the capability to establish thick recording layers. Among photopolymers, the ones based on polyvinil alcohol (PVA) matrix, and using acrylamide (AA) monomers have been extensively studied[5-6], as they combine good optical properties, ease of fabrication and self-development capability. Different models have been proposed to predict the performance of the photopolymer, based on the interplay between photopolymerization and diffusion. In the case of the PVA/AA compounds produced in our lab we find that even though diffusion is very slow, we have to take it into account to predict the correct evolution in time of the diffraction eficiency of our materials[7].

A great variety of formalisms, such as coupled wave, modal and perturbation theories, have been developed to study the interaction of incident illumination onto volume holograms[1,8]. In general, no analytical solutions exist and numerical methods have to be applied to calculate the diffraction efficiency. Fortunately, in many instances we can use the approximate Coupled Wave Theory proposed by Kogelnik[9,10] that assumes that only two orders propagate in the hologram. This theory provides a set of analytical solutions for the diffraction efficiency of the zero (transmitted) and the first diffracted orders, when a plane wave incides onto a sinusoidally periodic grating. Actually, the theory provides the expressions for the complex amplitude transmittance for the transmitted and the diffracted orders.

In the application of volume holography to optical information processing most of the work has been dedicated to Vander Lugt kind of filters, and in general to filters to be used in the Fourier plane of an optical processor[11]. A

* Tel.: +34-96-5903651; Fax: +34-96-5909750; E-mail: amarquez@dfists.ua.es

different strategy was proposed at the end of the 70s. dedicated to modify the impulse response of the optical system with no need for a Fourier plane[12-14]. The system is simple and compact: we simply need an imaging setup. This image processing strategy takes advantage of the characteristics of the angular response of the volume hologram that modifies the plane wave spectrum of the object. Following this strategy, image edge enhancement and image restoration were demonstrated. In recent years, the interest in this Bragg processing based operations has attracted the attention of researchers working with acousto-optic light modulators (AOLMs)[15-18]. In AOLMs, Bragg diffraction effects have been described using the frequency transfer function formalism. Using this formalism in combination with Kogelnik's expresssions we showed the application of PVA/AA photopolymers to edge enhancement by Bragg processing[19,20].

In general, optical processors are designed to implement space-invariant operations as in pattern recognition by optical correlation[21]. However, the Fourier transform itself is a space-variant operation[22,23]. A good review of the space-variant formalism and related applications can be found in Ref. 22-24. In general, optically performed space-variant operations are applied to optical interconnection or to coordinates transformations. Image processing operations have also been proposed[24-26] using volume holograms replayed in the Fourier plane of an optical processor. However, to our knowledge, no volume holograms have been used in space-variant image processing with no need for a Fourier plane.

Holographic optical elements[3,27] (HOEs) are diffractive optical elements[28] (DOEs), and therefore work by diffracting light from a generalized grating structure with nonuniform groove spacing. In the case of holographic lenses or (hololenses) the important parameters are the diffraction efficiency together with the generic parameters associated with the imaging capabilities of lenses, such as the compensation of aberrations. However, the hololens (and any other HOE) possess a local structure which is also interesting to be analysed. The usual approximation is to consider the HOE as a diffraction grating whose period varies along the surface of the HOE[29]. This local grating approximation enables to apply ray tracing methods to study the performance of the HOE[30]. Taking into account this local grating structure we could think of the HOE as a possible candidate to be applied as a filter for image processing operations with no need of a Fourier plane. As the grating structure varies with position we can deduce that space-variant operations may be possible.

In this work we demonstrate, to our knowledge for the first time, both theoretically and experimentally that a hololens can be used in space-variant filtering operations with no need for a Fourier plane. We will show space-variant edge enhanced images obtained experimentally in an imaging setup. For this purpose we introduce a hololens recorded on PVA/AA photopolymer. In Section 2 we derive the transfer functions for the transmitted and diffracted orders using Kogelnik's analytical solutions for an unslanted phase volume grating. We also introduce some considerations on space-variant systems. In Section 3 we analyse which parameters are involved in the design of a Bragg filter, focusing on the width of the passband of the filter. Some simulated results of image processing operations are given. In Section 4 we analyse the local structure of a hololens, and its reconstruction geometry. This enables to understand its space-variant properties when applied as a Bragg filter. In Section 5 some experimental results are given both with volume phase gratings, and with hololenses. Finally, in Section 6 the main conclusions of this work are summarised.

2. THEORY

2.1 Complex amplitude angular response

Recently we showed[19] that the analytical expressions from Kogelnik's theory provide an accurate description for the spatial filtering operations performed by holographic gratings. According to Kogelnik's theory[9], for a volume phase unslanted transmission grating the expressions for the transmitted R and the diffracted S wave amplitudes after passing through the hologram are,

$$R = \exp(-j\xi)\left(\cos\sqrt{\nu^2+\xi^2} + j\xi\, sinc\sqrt{\nu^2+\xi^2}\right) \tag{1}$$

$$S = \exp(-j\xi)(-j\nu) sinc\sqrt{\nu^2+\xi^2} \tag{2}$$

where $sinc(x) = sin(x)/x$ and,

$$\nu = \frac{\pi\,\Delta n\, d}{\lambda_0 \cos\theta_r'}\,;\xi = \frac{\pi d}{\Lambda\cos\theta_r'}\left(\left|sin\theta_r'\right| - \frac{\lambda_0}{2n_0\Lambda}\right) \tag{3}$$

n_0 and Δn are respectively the average and the modulation of the refractive index, d is the thickness of the medium, Λ is the period of the grating, λ_0 is the wavelength of reconstruction in air and θ_r' is the angle of reconstruction in the recording medium related to the angle of reconstruction in air θ_r by Snell's law. Bragg angle θ'_{Bragg} inside the material is

given by $sin\theta'_{Bragg} = \lambda_0/2n_0\Lambda$, thus ξ (eq. (3)) expresses deviation from the Bragg condition. The parameter ν expresses the amplitude of the phase modulation recorded in the volume grating. In holography, we note that usually intensity related magnitudes, such as diffraction efficiency, are sought. However, in Bragg processing we are actually interested in the complex amplitude expressions given by equations (1) and (2).

2.2 Transfer function formalism and space-variant systems

We can express the angular responses R and S, which depend on the angle θ_r of the incident beam with respect to the normal of the hologram, as frequency transfer functions. According to Figure 1, let us consider θ_o and ψ respectively as the angles of the plane wave spectrum of an input object and the orientation of the grating with respect to the optical axis in a certain optical system. Thus the angle θ_r is given by $\theta_r = \theta_o - \psi$, and the angular responses R and S of the grating modify the spectrum of plane waves propagating from the object. Similarly, equations (1) and (2) can be expressed as a function of the angular frequency p (rad/meter), given by $p = 2\pi sin\theta_o/\lambda_0$, to obtain the angular frequency transfer functions $H_0(p)$ and $H_1(p)$ for the zero and the first diffracted orders.

Interesting properties arise when the grating is oriented at $\psi = \theta_{Bragg}$, where θ_{Bragg} is the Bragg angle in air. We can make the transmitted order behave as a high-pass filter, whereas the diffracted order acts as a low-pass filter[18]. Using AOLMs, Davis et al.[18] have also shown that by changing the value of ν, it is possible to select the edges to be enhanced and the degree of enhancement. We have shown[19] this asymmetric edge enhancement using volume gratings recorded on PVA/AA photopolymer.

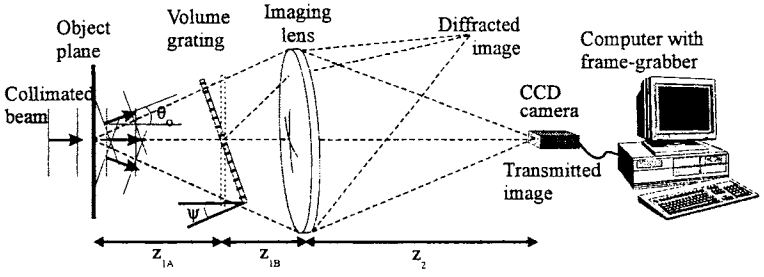

Figure 1. Imaging system with a volume grating. We show the deviation of the transmitted and the diffracted images by the grating.

Let us analyze the effect of the holographic grating inserted in an imaging setup as in Figure 1. We develop the expressions in one dimension. Extension to two dimensions is straightforward. The holographic grating is at distances z_{1A} and z_{1B} respectively from the object $f(x)$ and the lens, and z_2 is the image distance. When no grating is inserted, according to diffraction theory[11] the image amplitude $g(x')$ is given as the convolution ($\otimes$) of the object by the impulse response of the optical system $h_s(x')$,

$$g(x') = (f \otimes h_s)(x') \tag{4}$$

Using the convolution theorem we can rewrite equation (3) as,

$$G(p) = F(p)H_s(p) \tag{5}$$

where capitals represent the Fourier transform functions. When we introduce the holographic grating in the setup the angular frequency spectra of the object $F(p)$ is filtered respectively by the transfer functions $H_0(p)$ and $H_1(p)$ of the grating, thus we obtain two different filtered images,

$$G_0(p) = F(p)H_0(p)H_s(p) \; ; \; G_1(p) = F(p)H_1(p)H_s(p) \tag{6}$$

being $G_0(p)$ and $G_1(p)$ respectively the angular frequency contents for the transmitted and the diffracted images. We see that spatial filtering is performed with no physical Fourier plane.

Next we need to introduce some fundamentals about the linear systems formalism dealing with space-variant processing[22,23]. The equations (4)-(6) are valid for space-invariant systems. In the more general case of space-variant systems the impulse response varies along the object coordinate x, i.e. $h_s(x'; x)$, and we replace the convolution integral in equation (4) for a superposition integral,

$$g(x') = \int_{-\infty}^{+\infty} h_s(x'; x) f(x) dx \tag{7}$$

The convolution theorem is no longer valid and in principle the transfer function formalism can not be used. However, we can still consider that the space-invariance remains for small vicinities in the object plane. Following this approach the frequency transfer formalism can be used at the expense of using a different transfer function for each vicinity. We will see that this scheme will serve to explain the space-variant performance when we use the hololens as a filter in Bragg processing.

3. CHARACTERISTICS OF THE BRAGG FILTER

We want to analyze some specific trends exhibited by the transfer functions $H_0(p)$ and $H_1(p)$ derived from Kogelnik's theory in Section 2. To simulate the volume grating we consider typical values for a PVA/AA photopolymer grating with maximum diffraction efficiency: n_0 = 1.50, Δn = 0.003, d = 100 μm, Λ = 0.9 μm (1125 l/mm). For these values, at λ_0 = 633 nm, we obtain: θ_{Bragg}(in air)= ±20.8°. In Figure 2 we show the profile corresponding to the transfer functions for the transmitted (plots (a) and (b)) and the diffracted (plots (c) and (d)) orders. Plots (a) and (c) show the amplitude (modulus) and plots (b) and (d) show the phase. We consider the grating oriented at Bragg angle $\psi = \theta_{Bragg}$ and the frequency content is plotted as a function of the angle θ_o (in degrees) with respect to the optical axis of the imaging system (Figure 1).

If we look at the amplitudes in Figure 2(a) and (b), we see that $H_0(p)$ shapes a high-pass filter and $H_1(p)$ behaves like a low-pass filter respectively. In the vicinity of the origin the phase for the transmitted order (fig. 2 (b)) has the step profile typical of a derivative filter, changing from –90° to 90°. In the approximation to small angles we actually can see that the transfer function for the transmitted order becomes a derivative filter when the parameter ν is close to $\pi/2$[18] radians. We remind that when $\nu = \pi/2$ rad (at $\theta_r = \theta_{Bragg}$) a phase volume grating exhibits 100% diffraction efficiency[4].

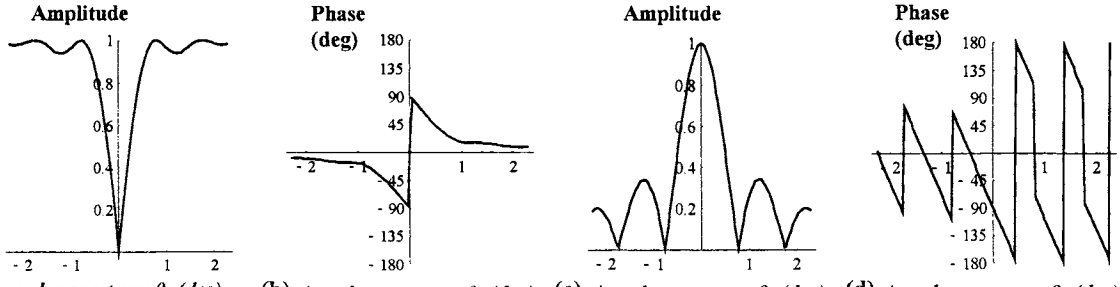

(a) *Angular spectrum θ_o (deg)* (b) *Angular spectrum θ_o (deg)* (c) *Angular spectrum θ_o (deg)* (d) *Angular spectrum θ_o (deg)*

Figure 2. (a) Transfer function (modulus) and (b) phase for the transmitted order. (c) Transfer function (modulus) and (d) phase for the diffracted order. The X axis is given as a function of the angle θ_o (scaled with λ_0 = 633 nm). Grating thickness is 0.1 mm.

Let us observe in Figure 3 an example of the resultant images produced by the filters given in Figure 2. We will consider an amplitude object. Results using a phase object have also been done[20]. Our input object is composed of two slits with different widths of *7 μm* and *70 μm* as can be seen in Fig. 3(a). In Figure 3(b) we plot the Fourier transform (modulus) of the object, scaled for illumination with a wavelength λ_0 = 633 nm. The frequency content is plotted as a function of the angle θ_o (in degrees) for the angular spectrum of the object, as in Figure 2. We observe the *sinc* behavior corresponding to a Fourier transformed rectangle function. Actually, we have the addition of the *sinc* functions for the two slits. Note that the angular interval (X-axis) has been amplified with respect to Figure 2. In Fig. 3(c) and 3(d) we show the transmitted and the diffracted images processed respectively by the filters $H_0(p)$ and $H_1(p)$. We see that the

result is different for the two slits. In the case of the wider slit (*70 μm*) the transmitted image (Fig. 3(c)) is an edge enhanced version of the input object, and the diffracted image (Fig. 3(d)) is a low-pass version where the edges have been smoothed. For the thinner slit (*7 μm*) we do not obtain any useful image processing operation: the transmitted image is a distorted version of the original slit, and in the diffracted order we just obtain a background noise along the *X*-axis.

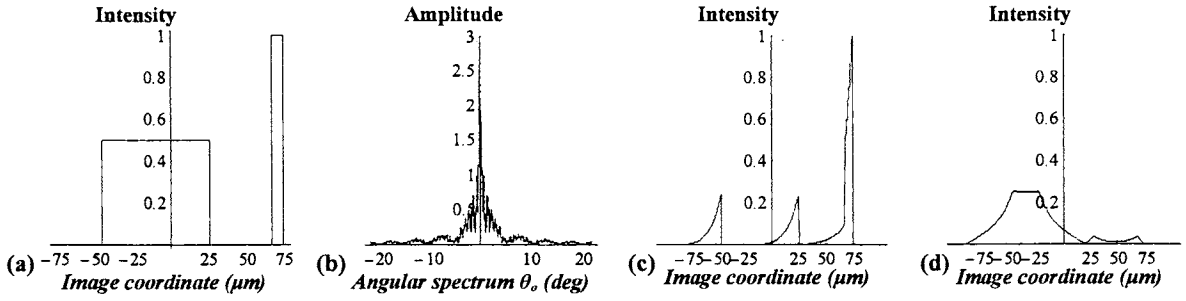

Figure 3. (a) Input object: two slits with a different width (*7 μm* and *70 μm*); (b) Frequency content of the object as a function of the angle θ_0 (scaled with λ_0 = 633 nm); (c) Transmitted image; (d) Diffracted image. Grating thickness is 0.1 mm.

The different performance of the filters for the two slits is due to the relative width of the passband of the filter with respect to the width of the frequency spectrum for each slit. The frequency spectrum of the thinner slit is much larger than the passband of the filter, thus the filter is not discriminating between low and high frequencies. We have found that the important parameter to control the passband of the filter is given by the product $Q\Lambda$, where Λ is the period of the grating and Q is the Klein-Cook parameter defined as,

$$Q = \frac{2\pi\lambda_0 d}{n_0 \Lambda^2} \tag{8}$$

where the magnitudes in equation (8) have already been introduced in the text. The Klein-Cook parameter expresses the degree of volume effects[4] exhibited by the grating. In general, small values of Q (Q<1) correspond to thin gratings, while large values (Q>1) correspond to volume gratings. We find that the width of the passband is inversely related with the magnitude of the product $Q\Lambda$. Thus, gratings with a larger product $Q\Lambda$ will have a narrower bandwidth and should be used with objects with a narrower frequency spectrum. In the case of the results obtained in Fig. 2 and 3 the values for the Q factor and for the product $Q\Lambda$ are 342 and 304 μm respectively.

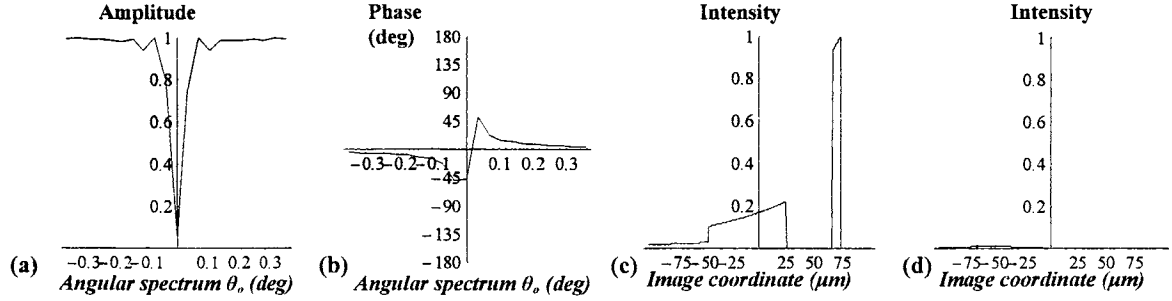

Figure 4. (a) Zero order transfer function (modulus) and (b) phase for the 1 mm thick grating;; (c) Transmitted image; (d) Diffracted image. Frequency contents in (a) and (b) are displayed as a function of the angle θ_0 (scaled with λ_0 = 633 nm).

Let us calculate the performance if we consider a filter at maximum diffraction efficiency and with a thickness d = 1 mm. The other parameters are left unchanged. This would correspond to values 3360 and 2988 μm respectively for the magnitudes Q and $Q\Lambda$. In Figure 4 we show the simulated results. In plots (a) and (b) we see the amplitude and phase for the filter $H_0(p)$. Note that the angular interval (X-axis) has been amplified by about a factor of 10 with respect to Figure 2. The passband of the filter is clearly reduced. Plots (c) and (d) show the transmitted and the diffracted resultant images respectively. Now, none of the two transmitted slits has been high-pass filtered. In the diffracted order we simply observe a low background noise in the region where the *70 μm* slit should be reproduced.

Finally, let us consider the effect of small desalignments of the grating, i.e. the grating is not oriented at Bragg angle. In Fig. 5(a) and 5(b) we plot respectively the amplitude and the phase for the zero order transfer function $H_0(p)$ when the grating is 0.5° out of Bragg incidence. In Fig. 5(c) and 5(d) we show respectively the transmitted and the diffracted resultant images. The simulation is done for a grating thickness $d = 0.1$ mm, as in Fig. 2 and 3. With just 0.5° of desalignment there is a dramatic change with respect to the images obtained in Fig. 3(c) and 3(d). Thus, any desalignment of the grating in the setup is clearly visible and can be easily corrected. Furthermore, we will see in the next Sections that the variation of the Bragg angle can also be used to perform space-variant operations as we demonstrate experimentally in Section 5 using hololenses.

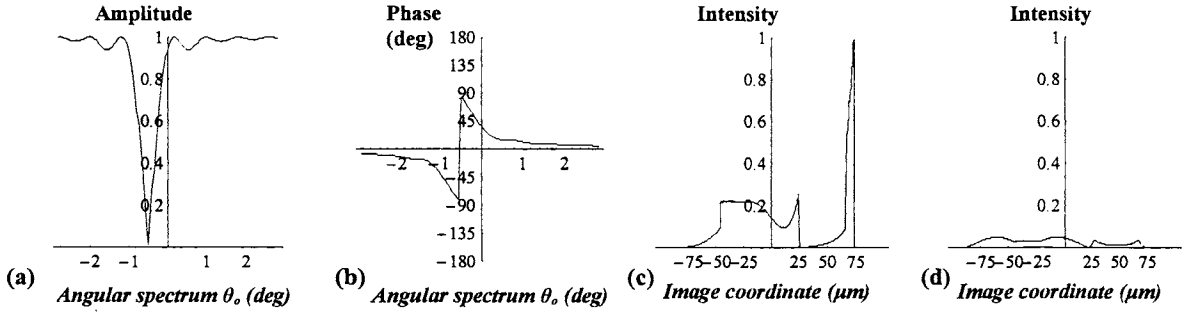

Figure 5. (a) Zero order transfer function (modulus) and (b) phase with the grating 0.5° out of Bragg incidence; (c) Transmitted and (d) diffracted images. Frequency contents are displayed versus the angle θ_o (scaled with $\lambda_0 = 633$ nm). Grating thickness is 0.1 mm.

4. LOCAL STRUCTURE OF THE HOLOLENS

In previous Sections we have analysed the performance of volume phase gratings in Bragg filtering image processing operations. This analysis can be generalized for more complex holographic optical elements. In this work we focus our attention in hololenses. To understand the performance of hololenses in Bragg filtering we first need to calculate its local structure.

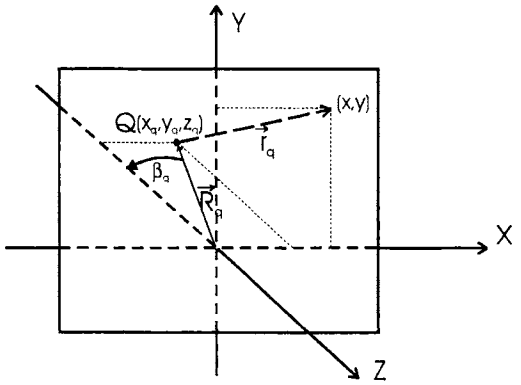

Figure 6. Geometry and notation used to calculate the recording of a hololens.

In Figure 6 we show the scheme for registering a hololens. A spherical wave front is generated at point Q with coordinates $\vec{R}_q = x_q\vec{i} + y_q\vec{j} + z_q\vec{k}$ with respect to the origin. For simplicity we consider point Q on the plane XZ. We call β_q the angle of the position vector $\vec{R}_q$ with respect to the Z-axis. We place the recording material in the plane $Z = 0$. To indicate the reference and the object wave fronts we substitute the generic subindex q by R or O respectively. According to this notation the wave vector $\vec{k}_q$ in air associated with the spherical wavefront at a point (x,y) on the surface of the hologram is given by,

$$\vec{k}_q(x,y) = \frac{2\pi}{\lambda_0}\frac{\vec{r}_q(x,y)}{r_q(x,y)} \tag{9}$$

, where $\vec{r}_q(x,y)$ corresponds to the vector with origin at the point Q. Refraction occurs at the interface between air and the medium, with index n_R. The following relations hold between the incident $\vec{k}_q$ and the refracted $\vec{k}'_q$ wave vectors,

$$k_{xq} = k'_{xq} \;\; ; \; k_{yq} = k'_{yq} \; ; \; k'_{zq} = \sqrt{\left(\frac{2\pi}{\lambda_q} n_R\right)^2 - k_{xq}^2 - k_{yq}^2} \tag{10}$$

, where we impose continuity of the transverse components at the interface. The reference $\vec{k}'_R$ and object $\vec{k}'_O$ wavefronts generate a set of interference (or Bragg) planes, characterized by the grating vector $\vec{K}_G$,

$$\vec{K}_G(x,y) = \vec{k}'_R(x,y) - \vec{k}'_O(x,y) \tag{11}$$

We consider the local grating approximation, i.e. the Bragg planes are equivalent along the depth of the material. As a consequence the grating vector $\vec{K}_G$ only depends on the x and y coordinates. As shown in Figure 7(a), the parameters associated with the structure of the recorded HOE are the grating period $\Lambda(x,y)$ and the Bragg plane orientation, where we consider the angle $\phi(x,y)$ with the Z-axis. We can calculate their values by means of the following relations,

$$\Lambda = \frac{2\pi}{K_G} \; ; \; sin\phi = \frac{K_{zG}}{K_G} \tag{12}$$

, where K_G and K_{zG} correspond to the modulus and to the Z-component of the grating vector $\vec{K}_G$ respectively.

Depending on the material that we use it can happen that the thickness and/or the index n_C of the material have changed when replaying the hologram in the reconstruction step. Furthermore, the reconstruction wavelength λ_C can be different from the one used in the registering step. In the case of our PVA/AA photopolymer we have found that the thickness and the index of refraction does not change.

To reconstruct the HOE in Bragg incidence, the reconstruction $\vec{k}'_C$ and the image (or diffracted) wave vectors $\vec{k}'_I$ have to fulfill the Bragg law at every point *(x, y)*,

$$\vec{K}_G(x,y) = \vec{k}'_C(x,y) - \vec{k}'_I(x,y) \tag{13}$$

From equation (12) and considering the scheme in Figure 7(b) we can calculate the Bragg angle. We will distinguish between the positive θ'_{+Bragg} and the negative θ'_{-Bragg} Bragg angles. The positive Bragg angle θ'_{+Bragg} corresponds to a reconstruction beam which incides along the direction of the reference beam, whereas by negative Bragg θ'_{-Bragg} we mean that the reconstruction beam incides along the direction followed by the object beam. We can calculate the magnitude of the Bragg angles inside of the material using the following expression,

$$\theta'_{\pm Bragg} = \frac{\varpi}{2} \pm \phi \tag{14}$$

, where ϖ is given by,

$$sin\left(\frac{\varpi}{2}\right) = \frac{K_G/2}{k'_C} \tag{15}$$

, and k'_C is the modulus of the reconstruction wave vector in the medium, i.e. $k'_C = (2\pi n_C)/\lambda_C$. We note that in the previous expressions the only approximation that we have applied is the local grating approximation. Thus, our derivations are valid both for paraxial and for non-paraxial incidence.

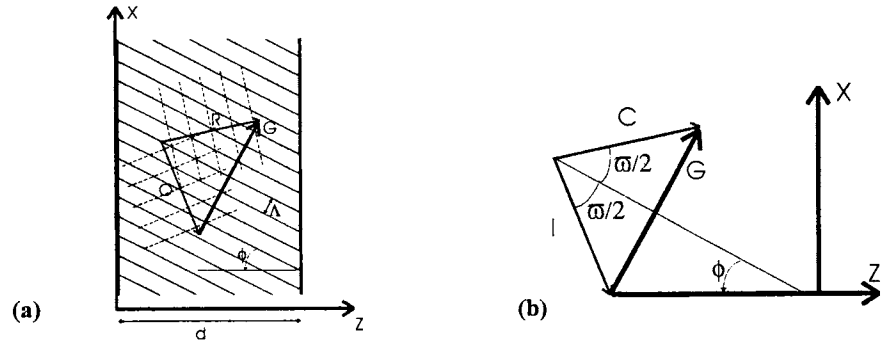

Figure 7. (a) Scheme of the parameters associated with the structure of the Bragg planes recorded in the material; (b) Geometry used to calculate the positive and the negative Bragg angles given in the text.

Using the previous expressions we calculate theoretically the local structure for some of the hololenses that we have produced on the PVA/AA photopolymer. In the registering step we use illumination with λ_R = 514 nm (Argon laser) with a collimated reference beam at an angle of incidence of 16.8° with respect to the normal of the hologram. The object beam originates at a point with polar coordinates $(R_O = 10\,cm, \beta_O = -16.8°)$. The diameter of the interference region on the material is 2 cm. Thus, we generate an off-axis hololens with a 10 cm focal length for the 514 nm wavelength and with a 2 cm diameter. In the reconstruction step we use a beam with a wavelength λ_C = 633 nm (He-Ne laser).

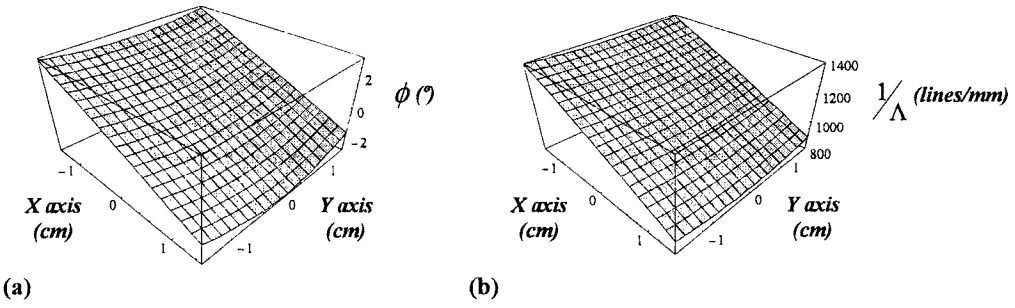

Figure 8. (a) Orientation and (b) period of the Bragg planes across the aperture of the hololens.

Using the local grating approximation approach it is interesting to note that the interference at coordinates *(0,0)* corresponds to the symmetrical geometry considered in the examples studied in Section 3. Out of this point we lose the symmetry between the incidence of the two wave vectors and we will generate slanted gratings with varying periods. In Figures 8(a) and (b) we show respectively the results for the orientation ϕ of the Bragg planes and their period Λ along the grating coordinates *X-Y* expressed in centimeters. In the area of the hololens (2 cm diameter) the orientation of the Bragg planes oscillates between 2° and –2°, whereas the spatial frequency (in lines/mm) covers a range of approx. 500 lines/mm. In the plots we observe the symmetry with respect to the coordinate $y = 0$.

In Figures 9(a) and (b) we show a contour plot respectively for the positive and the negative Bragg angle in air along the *X-Y* plane of the hologram. In the gray level legend of the figures we can see that the range of variation for the positive Bragg angle is between 22° and 19° approximately. In the case of the negative Bragg angle the variation is larger, ranging from –11° to –30°. At the center, coordinate *(0, 0)*, the Bragg angle is respectively +20.8° and –20.8° as in the examples in Section 3. The angle variation is much smaller in the case of the positive Bragg angle due to fact that in this case the reconstruction beam tries to replay the reference beam, which had a collimated wavefront.

Let us discuss the application of the hololens as a Bragg filter. As the Bragg angle varies across its aperture we can not talk about a global transfer function for the hololens, but we can imagine local transfer functions valid for a small vicinity in the object where we can consider space-invariance. We imagine the object windowed in these small vicinities, each one possessing its own plane waves spectrum. For a certain orientation of the hololens only one of these vicinities will satisfy that its zero frequency component incides at the Bragg angle. Thus, we can only have edge enhancement

(transmitted order) or low-pass filtering (diffracted order) for these particular vicinity in the object, whereas the rest of the object is left practically unchanged (as shown in Fig. 5). The rapidness of the Bragg angle variation will be responsible for the scale of the vicinities in the object: when we replay under the negative Bragg angle, then the spatial extent of the filtered area in the object is smaller than in the case of the positive Bragg angle. In Section 5 we will show the experimental images confirming these hypotheses.

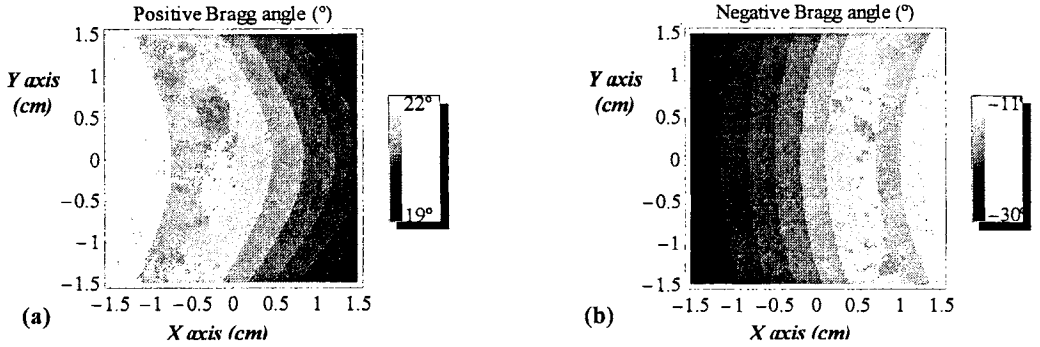

Figure 9. (a) Positive and (b) negative Bragg angles across the aperture of the hololens.

Finally, in Figure 10 we want to show the effect of the thickness of the hololens. Plot (a) and (b) correspond to the product $Q\Lambda$ for a thickness of 0.1 mm and 1 mm respectively. We see that the value of $Q\Lambda$ varies across the hologram, thus the width of the passband varies as well, as commented in Section 3. In the case with a thickness of 1 mm, we see that $Q\Lambda$ is very large and therefore we can only expect edge enhancement in the case of objects with a small frequency bandwidth.

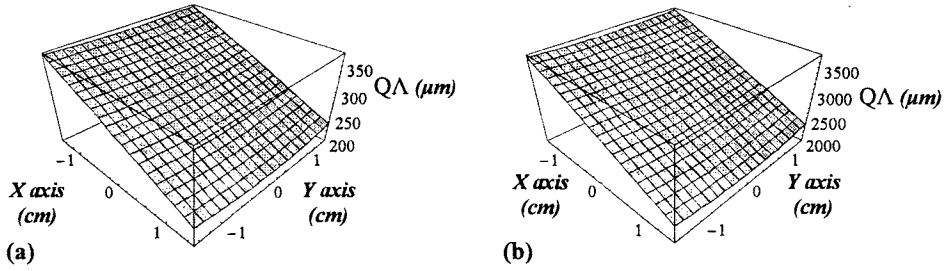

Figure 10. Product $Q\Lambda$ across the aperture of the hololens for a hologram thickness of (a) 0.1 mm and (b) 1 mm.

5. EXPERIMENTAL RESULTS

In the experiments a He-Ne laser beam (λ_0 = 633 nm) is spatially filtered, expanded, and collimated, serving as the source of illumination for an imaging setup (Figure 1), where we use a lens with a focal length f' = 15 cm and a clear aperture diameter of 7.5 cm. We capture the transmitted (zero order) image using a CCD camera, Hamamatsu C5403, and a frame-grabber, Matrox Meteor, connected to a personal computer. We have not applied any digital enhancement to the images, thus we discuss the actual outputs of the experiment.

In the setup we have introduced phase transmission gratings and hololenses recorded on a PVA/AA photopolymer (preparation and composition details in Ref. 6-7), exposed to the green line (514 nm) of an Argon laser. In the case of the gratings the two interfering beams form an angle of 16.8° with respect to the normal of the plate (symmetrical mount), and generate an interference pattern of 2 cm diameter with a spatial frequency of 1125 lines/mm. To generate the hololenses one of the beams is focused at a distance of 10 cm from the center of the hologram. The values for the rest of the parameters for the PVA/AA photopolymer are similar to the ones used in the simulations in Section 3. We have produced gratings and hololenses close to the maximum diffraction efficiency.

In Fig. 11(a) we see an image obtained using a volume phase grating with a thickness of approx. 0.1 mm. It corresponds to the transmitted image of a section of the USAF 1951 resolution target in negative (chrome on glass plate).

We can distinguish the edge enhancement of those edges exhibiting a vertical component, which is the direction of the interference fringes of the grating inserted in the setup. The width of the vertical bars is *70 μm*, as one of the two objects simulated in Section 3. In Fig. 10(b) and (c) we show the transmitted image of a slit with the grating at Bragg incidence and the grating 0.5° out of Bragg incidence respectively. We clearly observe that in Fig. 10(c) there is no edge enhancement: what we see is nearly equal as the image of the slit with no grating in the setup.

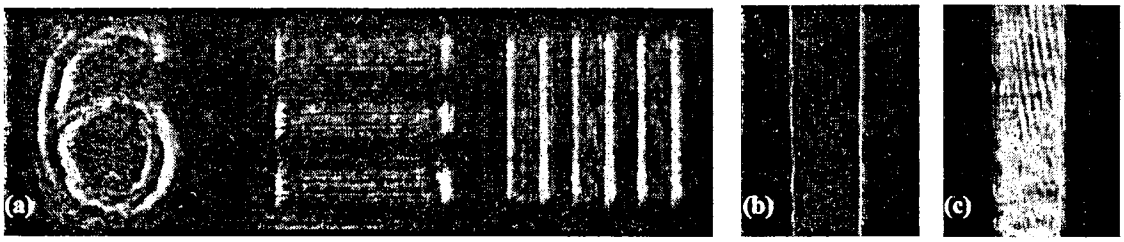

Figure 11. Phase volume grating. (a) Transmitted image of the USAF test target; Transmitted images of a *70 μm* slit with (b) the grating at Bragg incidence and, (c) the grating 0.5° out of Bragg incidence.

In the next figures (Fig. 12, 13 and 14) we will show some experimental images obtained using the hololens as a Bragg filter. The images correspond to an area of approx. *9x7* mm in the object. In all the cases we consider the transmitted image, i.e. the zero diffraction order. We can distinguish two different situations for the orientation of the hololens: the direction of the optical axis of the imaging setup is in the range of the positive Bragg angle of incidence, or is in the range of the negative Bragg angle.

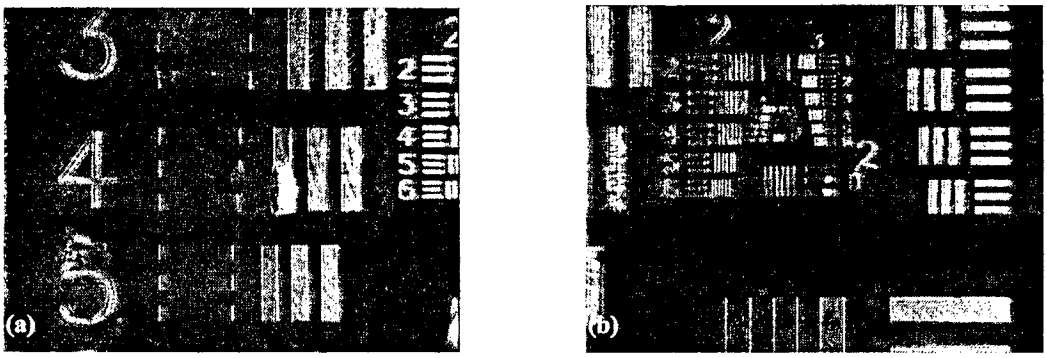

Figure 12. Zero order (transmitted) images obtained with the *0.1 mm* thick hololens. (a) and (b) correspond to two different orientations of the hololens at *positive* Bragg angle incidence.

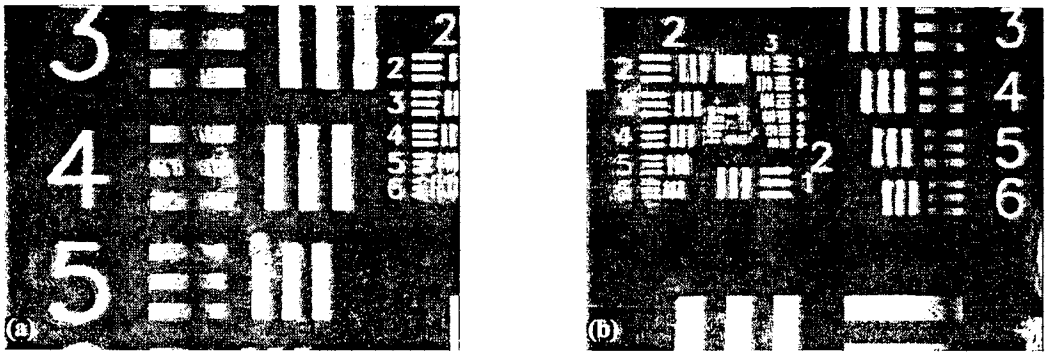

Figure 13. Zero order (transmitted) images obtained with the *0.1 mm* thick hololens. (a) and (b) correspond to two different orientations of the hololens at *negative* Bragg angle incidence.

In Figure 12 we show two images obtained using a hololens with a thickness of 0.1 mm oriented in the range of the positive Bragg angles. Images (a) and (b) correspond to two different orientations of the hololens (we rotate the hololens about the $x = 0$ axis) without moving the object (USAF 1951 resolution target). We shift the position of the CCD camera in order to capture the area of interest in the image in each case. We see that about a third part of images (a)

and (b) is edge enhanced, whereas the rest of the image has been transmitted without any filtering. We observe that the right side (corresponding to the Group 2 of the resolution target) of image (a) has not been affected by the hololens. However, after rotating very slightly the hololens (tenths of degree), now in image (b) this part of the object is edge enhanced.

In Figure 13 we use the same hololens as in Fig. 12 but now it is oriented in the range of the negative Bragg angles. Both in Fig. 13(a) and (b) we appreciate a narrow dark fringe crossing the image in the vertical direction. We saturated the illumination to increase the contrast of the fringe. As in Fig. 12, we can progressively move the position of this fringe with a slight rotation of the hololens. The dark fringe is due to the removing of frequencies in the selected area of the object. This energy is sent to the diffracted order. In principle, we do not appreciate edge enhancement, even though in image (b) it seems that the left edge of the horizontal bars could be edge enhanced. It is interesting to note that the width of the selected area of the object in the case of the negative Bragg angle orientation is clearly smaller than for the positive Bragg angle orientation. This is consistent with the fact that the Bragg angle varies more rapidly in the case of the negative Bragg orientation (as given in Fig. (9)).

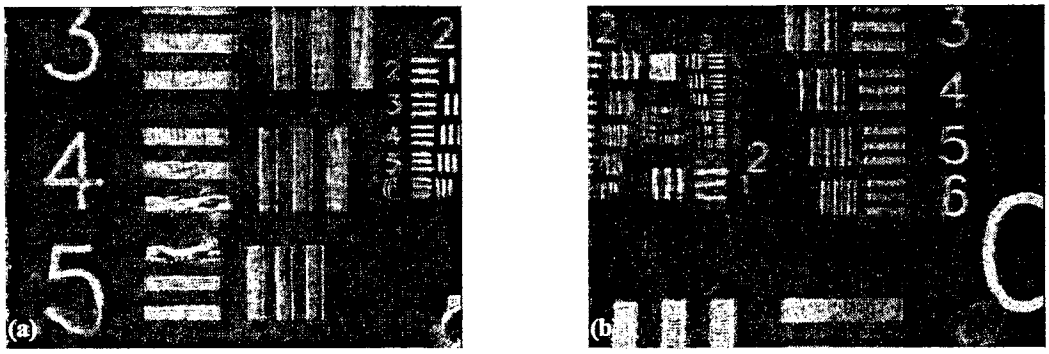

Figure 14. Zero order (transmitted) images obtained with the *1 mm* thick hololens. (a) and (b) correspond to two different orientations of the hololens at *positive* Bragg angle incidence.

Finally, in Figure 14 we show some results with a hololens with a thickness of about 1 mm and for the positive Bragg angle incidence. In (a) and (b) we see edge enhancement in a wide area of the images. The rapidness of the Bragg angle variation along the plane of the hololens is independent of the thickness of the material, thus the extent of the selected areas should be equal between the hololenses of 0.1 mm and 1 mm. Some extra experimental work should be done on these assumptions. In Fig. 14 the degree of edge enhancement is not as contrasted as in Fig. 12. We may think in two possibilities. First, the modulation parameter ν could be closer to $\pi/2$ in Fig. 12 than in Fig. 14. Second, if we take into account the product $Q\Lambda$ (simulations in Fig. (4) and Fig. (10)), we could also think that the passband is very narrow for the thicker hololens, and is not well adapted to edge enhance the small objects. As a final comment, images in Fig. 14 show more inhomogeneities (such as distorsion in number 5 in image (a)) than in Fig. 12. We should take into account that the thickness of the material is now very large, thus increasing the probability of fluctuations in its properties.

6. CONCLUSIONS

We have analysed the properties exhibited by volume phase gratings and holographic lenses when applied to image processing by Bragg filtering. We have simulated, using the analytical expressions from Kogelnik's theory, the performance of the Bragg filter to derive its main properties, such as sensitivity to Bragg incidence misalignment and sensitivity to the width of the passband of the filter. We have also modeled the local structure of the hololens applying the local grating approximation. This allowed us to calculate the variation of the Bragg angle along the plane of the hololens. We have generated hololenses with thicknesses of 0.1 and 1 mm on a PVA/AA photopolymer. Experimentally we have proved space-variant edge enhancement using the hololens. Rotation of the hololens allows the selection of different areas in the object. We also verified the smaller extent of the filtered area when the Bragg angle varies more rapidly across the aperture of the hololens.

ACKNOWLEDGMENTS

This work has been partially financed by Ministerio de Ciencia y Tecnología, Spain, project MAT2000-1361-C04-04, and by Generalitat Valenciana, Spain, project GV01-130.

REFERENCES

1. R. R. A. Syms, *Practical Volume Holography*, Clarendon Press, Oxford (1990).
2. H.J. Coufal, D. Psaltis and B.T. Sincerbox, eds., *Holographic data storage*, Springer-Verlag, Berlin (2000).
3. T.W. Stone and B.J. Thompson, eds., *Selected Papers on holographic and diffractive lenses and mirrors*, SPIE Milestone Series, Vol. MS 34 (1991).
4. P. Hariharan, *Optical Holography*, Cambridge University Press, Cambridge, (1996).
5. S. Blaya, L. Carretero, R. Mallavia, A. Fimia, R. F. Madrigal, M. Ulibarrena and D. Levy, "Optimization of an acrylamide-based dry film used for holographic recording", *Appl. Opt.* **37**(32), 7604-7610 (1998).
6. M. Ortuño, S. Gallego, C. García, C. Neipp, A. Beléndez and I. Pascual, "Optimization of a 1 mm thick PVA/acrylamide recording material to obtain holographic memories: method of preparation and holographic properties", *Applied Physics B* **76**, 851-857 (2003).
7. C. Neipp, S. Gallego, M. Ortuño, A. Márquez, M.L. Álvarez, A. Beléndez and I. Pascual, "First-harmonic diffusion-based model applied to a polyvinyl-alcohol-acrylamide-based photopolymer", *JOSA B* **20**, 2052-2060 (2003).
8. T. K. Gaylord and M. G. Moharam, "Analysis and applications of optical diffraction by gratings", *Proc. IEEE* **73**(5), 894-937 (1985).
9. H. Kogelnik, "Coupled wave theory for thick hologram gratings", *Bell Syst. Technol. J.* **48**(9), 2909-2947 (1969).
10. C. Neipp, I. Pascual and A. Beléndez, "Theoretical and experimental analysis of overmodulation effects in volume holograms recorded on BB-640 emulsions", *J. Opt. A: Pure Appl. Opt.* **3**, 504-513 (2001).
11. J. W. Goodman, *Introduction to Fourier Optics*, McGraw-Hill, 2nd edition, New York, (1996).
12. S. K. Case, "Fourier processing in the object plane", *Opt. Lett.* **4**(9), 286-288 (1979).
13. D. Peri and A. A. Friesem, "Image restoration using volume diffraction gratings", *Opt. Lett.* **3**(4), 124-126 (1978).
14. D. Peri and D. Ritter, "Spatial filtering with volume gratings", *Appl. Opt.* **24**(10), 1535-1540 (1985).
15. J. Xia, D. B. Dunn, T.-C. Poon and P. P. Banerjee, "Image edge enhancement by Bragg diffraction", *Opt. Commun.* **128**, 1-7 (1996).
16. D. Cao, P. P. Banerjee and T.-C. Poon, "Image edge enhancement with two cascaded acousto-optics cells with contrapropagating sound", *Appl. Opt.* **37**(14), 3007-3014 (1998).
17. P. P. Banerjee, D. Cao and T.-C. Poon, "Notch spatial filtering with an acousto-optic modulator", *Appl. Opt.* **37**(32), 7532-7537 (1998).
18. J. A. Davis and M. D. Nowak, "Selective edge enhancement of images with an acousto-optic light modulator", *Appl. Opt.* **41**(23), 4835-4839 (2002).
19. A. Márquez, C. Neipp, S. Gallego, M. Ortuño, A. Beléndez and I. Pascual, "Edge enhanced imaging using PVA/acrylamide photopolymer gratings", *Opt. Lett.* **28**(17), 1510-1512 (2003).
20. A. Márquez, C. Neipp, S. Gallego, M. Ortuño, A. Beléndez and I. Pascual, "Analysis of Bragg diffraction filters applied to image processing", sent for publication to Physica Scripta.
21. J. Campos, A. Márquez, M. J. Yzuel, J. A. Davis, D. M. Cottrell and I. Moreno, "Fully complex synthetic discriminant functions written onto phase-only modulators", *Appl. Opt.* **39**, 5965-5970 (2000).
22. J. W. Goodman, "Linear Space-Variant Optical Data Processing", in *Optical Data Processing, Fundamentals*, ed. by S. Lee, pp. 235-260, Springer-Verlag, New York (1981).
23. W. T. Rhodes, "Space-Variant Optical Systems and Processing", in *Applications of the Optical Fourier Transform*, ed. by F. Stark, pp. 333-369, Academic Press, New York (1981).
24. J. F. Walkup, "Space-variant coherent optical processing", *Opt. Eng.* **19**(3), 339-346 (1980).
25. R. Kasturi, T. F. Krile and J. F. Walkup, "Multiplex holography for space-variant processing: a transfer function sampling approach", *Appl. Opt.* **20**(5), 881-886 (1981).
26. P. Ambs, Y. Fainman, S. H. Lee and J. Gresser, "Computerized design and generation of space-variant holographic filters. 1: System design considerations and applications of space-variant filters to image processing", *Appl. Opt.* **27**(22), 4753-4760 (1988).
27. D. H.Close, "Holographic optical elements", *Opt. Eng.* **14**(5), 408-419 (1975).
28. J. Turunen and F. Wyrowski, *Diffractive optics for industrial and commercial applications*, Akademie Verlag, Berlin (1997).
29. A. Beléndez, I. Pascual and A. Fimia, "Optimization of reconstruction geometry for maximum diffraction efficiency in HOE – the influence of recording material", *Optica Applicata* **21**(3), 225-237 (1991).
30. J. N. Latta, "Computer-based analysis of holography using ray tracing", *Appl. Opt.* **10**(12), 2698-2710 (1971).